Individual pitch control by convex economic model predictive control for wind turbine side-side tower load alleviation

AK Pamososuryo[1], Y Liu[1], TG Hovgaard[2], R Ferrari[1], and JW van Wingerden[1]

[1]Delft Center for Systems and Control, Faculty of Mechanical Engineering, Delft University of Technology, Mekelweg 2, 2628 CD Delft, The Netherlands
[2]Vestas Technology R & D, Vestas A/S, Denmark

E-mail: A.K.Pamososuryo@tudelft.nl

Abstract. The wind turbine side-side tower motion is known to be lightly damped. One viable active damping solution is realized by deploying individual pitch control (IPC) such that counteracting blade forces are created to alleviate the tower fatigue loading caused by this motion. Existing IPC methods for side-side tower damping in the literature, such as linear quadratic regulator and lead-lag controller, cannot accommodate direct optimization and trade-off tunings of the wind turbine economic performance. In this work, a novel side-side tower damping IPC strategy under a convex economic model predictive control (CEMPC) framework is therefore developed to address these challenges. The main idea of the framework lies in the variable transformation in power and energy terms to obtain linear dynamics and convex constraints, over which the economic performance of the wind turbine is maximized with a globally optimal solution in a receding horizon manner. The effectiveness of the proposed method is showcased in a high-fidelity simulation environment under both steady and turbulent wind cases. Lower fatigue damage on the side-side tower bending moment is attained with an acceptable level of pitch activities, negligible impact on the blade loads, and minor improvement on the power production.

1. Introduction

Wind turbines are manufactured in record-breaking sizes to further decrease the levelized cost of energy by harnessing more power from the wind [1]. As wind turbine towers become ever taller, their wall thickness is typically decreased to maintain the cost of energy low, which consequently aggravates the fatigue loadings due to the increased structural flexibility [2]. From the control engineering perspective, this implies that load mitigation objectives are of even higher importance to ensure prolonged wind turbine operation—urging advanced control methods to be deployed.

Among the most prominent loads is that of the side-side tower since it is lightly damped. In addition, only negligible effects of the so-called aerodynamic damping is experienced, in contrast to the fore-aft motion [3]. In recent years, the most common control strategy used to mitigate prolonged side-side tower oscillation is the active damping by generator torque, such as the work done by Mulders, et al. [4] and references therein. Although proven to be effective, power

production can be affected as a side product of the load reduction activity, as demonstrated by Mulders, et al.

Alternatively, one may resort to the individual pitch control (IPC) to manipulate the blade in-plane forces' horizontal component; resulting in the side-side tower-top force counteracting the structural excitation [5]. The literature shows that the industry has been adopting this approach since nearly two decades ago [6]. Several academic studies emerged afterward, for instance, the work of Stol, et al. [7], which incorporates linear quadratic regulation approach and Duckwitz and Geyler [5], where a conventional lead-lag controller was designed. These methods, however, do not accommodate direct optimization and trade-off tunings of the wind turbine economic performance, such as power capture maximization, structural fatigue mitigation, and actuator activities penalization.

One of the state-of-the-art control methods capable of handling such requirements is the economic model predictive control (EMPC) [8, 9, 10]. EMPC operates by generating control inputs to maximize a system's economic performance formalized in the so-called optimal control problem (OCP) up to certain time steps in the future in a receding horizon manner. In wind turbine applications, however, EMPC often suffers from nonlinearities, such as those coming from the aerodynamics. This renders the OCP harder to solve, not to mention that a globally optimal solution cannot be guaranteed. To address these challenges, a novel convex economic model predictive control (CEMPC) strategy has been developed by Hovgaard, et al. [9] with the main goal to enable smooth power delivery to the grid. In this work, a power-and-energy-based variable transformation is conducted to allow linear dynamics and convex constraints to be incorporated in the CEMPC. Shaltout, et al. [10] have successfully integrated tower fore-aft damping objective into the framework and thereby exhibits the applicability of CEMPC for load mitigation. Unfortunately, to the best of our knowledge, the side-side tower load mitigation and individual pitching potentials of this framework have received little to no attention in the literature.

Therefore, our main focus in this study was to formulate an extension to the CEMPC framework of Hovgaard, et al. [9], accounting for the aforementioned side-side tower fatigue load reduction by means of IPC. In detail, this extension is made possible by augmenting a second-order wind turbine tower model with the tower-top force formulated in terms of aerodynamic powers and rotational kinetic energy to obtain linear tower dynamics.

The remainder of this paper proceeds as follows. In Section 2, the nominal wind turbine model is introduced, which is then reformulated in power and energy terms in Section 3. Section 4 elaborates the CEMPC implementation, including the OCP design and a brief discussion regarding the complementary state estimators. Simulation results and discussions are provided in Section 5. In Section 6, the conclusions of this work are given.

2. Nominal Wind Turbine Model

This section presents the derivation of the nominal wind turbine dynamical model comprised of the drivetrain and the side-side tower motion. To model the drivetrain dynamics, a one-mass model torque balance equation in continuous time t is employed as follows

$$J_{\mathrm{hss}}\dot{\omega}_{\mathrm{g}}(t) = T_{\mathrm{r}}(t)/G - T_{\mathrm{g}}(t)\,, \tag{1}$$

with the high-speed shaft equivalent inertia denoted by J_{hss} and the gearbox ratio by G. The generator speed ω_{g} and the generator torque T_{g} are operated within the following limits

$$\omega_{\mathrm{g,min}} \leq \omega_{\mathrm{g}}(t) \leq \omega_{\mathrm{g,max}}\,, \tag{2}$$

$$0 \leq T_{\mathrm{g}}(t) \leq T_{\mathrm{g,max}}\,, \tag{3}$$

where the subscripts 'min' and 'max' indicate the lower and upper bounds of the specified quantities.

The rotor aerodynamic torque T_{r} in (1) is defined as the total torque contribution of the individual blades [5, 11] as shown below

$$T_{\mathrm{r}}(t) = \sum_{i=1}^{B} T_{\mathrm{r},i}(t)\,, \tag{4}$$

where i being the blade index and $B = 3$ as the number of blades of the wind turbine under study. The individual blade aerodynamic torque $T_{\mathrm{r},i}$ is related to the individual aerodynamic power $P_{\mathrm{r},,i}$ by the following expression

$$T_{\mathrm{r},i}(t) = P_{\mathrm{r},i}(t)/\omega_{\mathrm{r}}(t)\,, \tag{5}$$

in which

$$P_{\mathrm{r},i}(t) = (1/2B)\rho A C_{\mathrm{p}}(\beta_i(t), \lambda_i(t))v_i(t)^3\,, \tag{6}$$

where ρ and A are the air density and the rotor area, respectively. The power coefficient C_{p} is a function of the individual pitch angle β_i, limited under the following bounds

$$\beta_{\min} \leq \beta_i(t) \leq \beta_{\max}, \quad i \in \{1, 2, 3\}\,, \tag{7}$$

and the tip-speed ratio $\lambda_i(t) = \omega_{\mathrm{r}}(t)R/v_i(t)$, with $\omega_{\mathrm{r}}(t) = \omega_{\mathrm{g}}(t)/G$ as the rotor speed, R as the rotor radius, and v_i as the blade-effective wind speed. This power coefficient is often represented as a look-up table whose values can be derived either numerical- or empirically.

At the generator side of the drivetrain, the generated power is obtained as the product of the generator speed and torque, taking into account the efficiency factor $\eta_{\mathrm{g}} \in [0, 1]$, as follows

$$P_{\mathrm{g}}(t) = \eta_{\mathrm{g}}\omega_{\mathrm{g}}(t)T_{\mathrm{g}}(t)\,, \tag{8}$$

which is restricted by the constraints

$$0 \leq P_{\mathrm{g}}(t) \leq P_{\mathrm{g,max}}\,. \tag{9}$$

To model the support structure, a second-order cantilever beam is employed to approximate the wind turbine side-side tower dynamics, where an acting force on its top is considered

$$M\ddot{x}_{\mathrm{ss}}(t) + D\dot{x}_{\mathrm{ss}}(t) + Kx_{\mathrm{ss}}(t) = F_{\mathrm{ss}}(t)\,. \tag{10}$$

The quantities $\ddot{x}_{\mathrm{ss}}$, $\dot{x}_{\mathrm{ss}}$, and x_{ss} in the above equation are referring to the tower acceleration, velocity, and displacement, respectively, and the symbols M, D, and K are designated as the first tower modal mass, damping, and stiffness coefficients. The side-side tower-top force F_{ss} is considered as the sum of its individual components $F_{\mathrm{ss},i}$, defined as the horizontal projection of the in-plane blade force $F_{\mathrm{ip},i}$. This mapping is formulated in the following equation

$$F_{\mathrm{ss}}(t) = \sum_{i=1}^{B} F_{\mathrm{ss},i}(t) = \sum_{i=1}^{B} -F_{\mathrm{ip},i}(t)\cos\left(\psi_i(t)\right), \tag{11}$$

where the i-th blade azimuth position is denoted by $\psi_i(t) = \psi(t) + 2\pi(i-1)/3$ with $\psi(t) = \omega_{\mathrm{r}}(t)t$ as the first blade azimuth position. The zero value of ψ is defined at its vertically upward position and increments in the clockwise direction as illustrated in Figure 1. Note that due to this convention, a negative sign precedes $F_{\mathrm{ip},i}$ in (11) due to the sign difference between the side-side force and the tower motion.

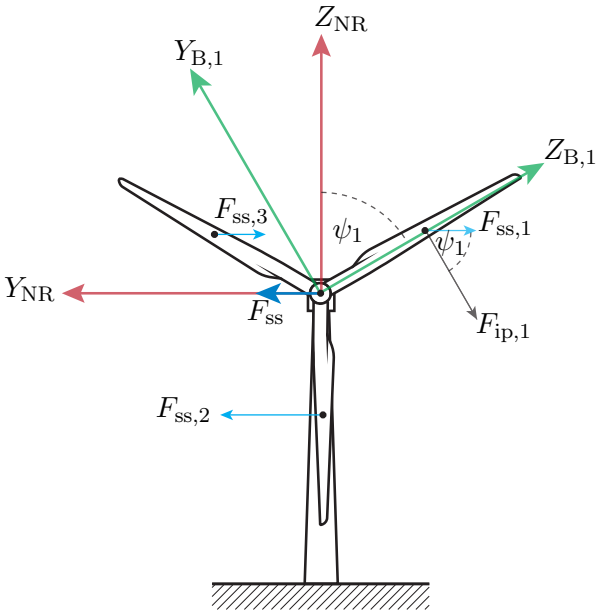

Figure 1: The in-plane force $F_{\mathrm{ip},i}$, only shown for the first blade, is perpendicular to the blade and acts at a $s_{\mathrm{c}}R$ distance away from the rotor center. Its horizontal component $F_{\mathrm{ss},i}$ is mapped by the azimuth ψ_i, which is created by the angular difference between the non-rotating (red arrows) and rotating (green arrows) reference systems. The side-side force F_{ss}, resulting from the summation of the individual horizontal blade forces, is shown to act on the tower-top.

The in-plane force acts perpendicularly to the corresponding blade at $s_{\mathrm{c}}R$ distance away from the rotor center to produce the individual aerodynamic torque $T_{\mathrm{r},i}$, with $s_{\mathrm{c}} = 1/2$ for a uniformly distributed force along the blade [11], formulated as

$$F_{\mathrm{ip},i}(t) = T_{\mathrm{r},i}(t)/s_{\mathrm{c}}R\,. \tag{12}$$

Having the nominal model and constraints derived above, the following remarks are laid out. First, the aerodynamic power, defined in (6), is a nonlinear function of the state ω_{g}, control input β_i, and disturbance v_i, and appears in both the dynamics of the drivetrain in (1) and tower in (10). Moreover, the generated power output formulated in (8) is a bilinear function of the state ω_{g} and control input T_{g}. Thus, it can be inferred that the nominal wind turbine model possesses dynamics and constraints nonlinear/nonconvex in its variables, the former of which can be represented as the following nonlinear state-space

$$\begin{cases} \dot{\mathbf{x}}(t) = f(\mathbf{x}(t), \mathbf{u}(t), \mathbf{d}(t)) \\ \mathbf{y}(t) = g(\mathbf{x}(t), \mathbf{u}(t), \mathbf{d}(t)) \end{cases}. \tag{13}$$

The states, inputs, disturbances, and outputs of the above equation are $\mathbf{x}(t) = [\omega_{\mathrm{g}}(t), \dot{x}_{\mathrm{ss}}(t), x_{\mathrm{ss}}(t)]^\top$, $\mathbf{u}(t) = [\beta_1(t), \beta_2(t), \beta_3(t), T_{\mathrm{g}}(t)]^\top$, $\mathbf{d}(t) = [v_1(t), v_2(t), v_3(t)]^\top$, and $\mathbf{y}(t) = [\omega_{\mathrm{g}}(t), P_{\mathrm{g}}(t), \ddot{x}_{\mathrm{ss}}(t)]^\top$, respectively. These nonlinear-/nonconvexity will pose additional challenges to model predictive control designs. One possible solution to tackle such an issue is by reformulating the dynamics and constraints linear/convex in their variable, e.g., by linearization. Alternatively, one may present a different set of variables such that the dynamics and constraints are linear/convex. The latter approach is taken into account in this work and treated in the next section.

3. Transformed Wind Turbine Model

In the model predictive control design of Hovgaard, et al. [9], the nonlinearity/nonconvexity issues of incorporating the nominal wind turbine dynamics are tackled by introducing the following variable transformations:

$$\begin{cases} \mathbf{x}(t) = [\omega_{\mathrm{g}}(t), \dot{x}_{\mathrm{ss}}(t), x_{\mathrm{ss}}(t)]^\top \\ \mathbf{u}(t) = [\beta_1(t), \beta_2(t), \beta_3(t), T_{\mathrm{g}}(t)]^\top \\ \mathbf{d}(t) = [v_1(t), v_2(t), v_3(t)]^\top \\ \mathbf{y}(t) = [\omega_{\mathrm{g}}(t), P_{\mathrm{g}}(t), \ddot{x}_{\mathrm{ss}}(t)]^\top \end{cases} \rightarrow \begin{cases} \mathbf{x}_{\mathrm{t}}(t) = [K_{\mathrm{g}}(t), \dot{x}_{\mathrm{ss}}(t), x_{\mathrm{ss}}(t)]^\top \\ \mathbf{u}_{\mathrm{t}}(t) = [P_{\mathrm{r},1}(t), P_{\mathrm{r},2}(t), P_{\mathrm{r},3}(t), P_{\mathrm{g}}(t)]^\top \\ \mathbf{d}_{\mathrm{t}}(t) = [v_1(t), v_2(t), v_3(t)]^\top \\ \mathbf{y}_{\mathrm{t}}(t) = [K_{\mathrm{g}}(t), P_{\mathrm{g}}(t), \ddot{x}_{\mathrm{ss}}(t)]^\top \end{cases}, \tag{14}$$

where power and energy terms are used, such that linear dynamics and convex constraints are obtained. The derivation of these dynamics and constraints is presented below.

Here, $K_{\mathrm{g}}(t) = (J_{\mathrm{hss}}/2)\omega_{\mathrm{g}}(t)^2$ is the rotational kinetic energy of the generator constrained by

$$(J_{\mathrm{hss}}/2)\omega_{\mathrm{g,min}}^2 \leq K_{\mathrm{g}}(t) \leq (J_{\mathrm{hss}}/2)\omega_{\mathrm{g,max}}^2\,, \tag{15}$$

derived straightforwardly from (2). The rate-of-change (ROC) of K_{g} is obtained by taking its first time-derivative and yields the following linear dynamics, substituting that of the drivetrain

$$\dot{K}_{\mathrm{g}}(t) = J_{\mathrm{hss}}\dot{\omega}_{\mathrm{g}}(t)\omega_{\mathrm{g}}(t) = \left(\sum_{i=1}^{B} T_{\mathrm{r},i}(t)/G - T_{\mathrm{g}}(t)\right)\omega_{\mathrm{g}}(t) = \sum_{i=1}^{B} P_{\mathrm{r},i}(t) - P_{\mathrm{g}}(t)/\eta_{\mathrm{g}}\,, \tag{16}$$

which are linear in their inputs.

The aerodynamic power $P_{\mathrm{r},i}$ is constrained by

$$0 \leq P_{\mathrm{r},i}(t) \leq \hat{P}_{\mathrm{av},i}(v_i(t), K_{\mathrm{g}}(t)), \quad i = \{1, 2, 3\}\,, \tag{17}$$

with

$$\hat{P}_{\mathrm{av},i}(v_i(t), K_{\mathrm{g}}(t)) = \min\{a_1 K_{\mathrm{g}}(t) + b_1, \ldots, a_j K_{\mathrm{g}}(t) + b_j\} v_i(t)^3\,, \tag{18}$$

as the piecewise linear (PWL) function approximation of the available power in the wind $P_{\mathrm{av},i}(v_i(t), K_{\mathrm{g}}(t)) = \max_{\beta_{\min} \leq \beta_i(t) \leq \beta_{\max}} (1/2B)\rho A C_{\mathrm{p}}(\beta_i(t), \lambda_i(t)) v_i(t)^3$, where a_m and b_m, with $m \in \{1, \ldots, j\}$, are the PWL function coefficients. It is important to note that the pitch limits in (7), as well as the wind speed information v_i, are now embedded in the above constraints.

To express the generated power bounds convex in the new variables, the constraints in (9) are rewritten as follows [10]

$$0 \leq P_{\mathrm{g}}(t) \leq \underbrace{\min\left(\eta_{\mathrm{g}}\sqrt{2K_{\mathrm{g}}(t)/J_{\mathrm{hss}}}T_{\mathrm{g,max}}, P_{\mathrm{g,rated}}\right)}_{P_{\mathrm{g,max}}}, \tag{19}$$

which is convex in P_{g} and concave in K_{g}.

Regarding the side-side tower dynamics, the tower-top force F_{ss} defined in (11) now needs to be reformulated as a function of the new variables. This is done firstly by substituting (5) into the in-plane force calculation (12) such that $F_{\mathrm{ip},i}(t) = P_{\mathrm{r},i}(t)/s_{\mathrm{c}}\omega_{\mathrm{r}}(t)R$. With $\omega_{\mathrm{r}}(t) = \sqrt{2K_{\mathrm{g}}(t)/J_{\mathrm{hss}}}/G$, further substituting $F_{\mathrm{ip},i}$ into (11) results in the new expression for the side-side force as follows

$$F_{\mathrm{ss}}(t) = \sum_{i=1}^{B} -\frac{P_{\mathrm{r},i}(t)}{s_{\mathrm{c}}\left(\sqrt{2K_{\mathrm{g}}(t)/J_{\mathrm{hss}}}/G\right)R}\cos\left(\psi_i(t)\right). \tag{20}$$

It can be noticed directly that F_{ss} contains the $1/\sqrt{K_{\mathrm{g}}}$ and $\cos(\psi_i)$ terms, which are nonconvex in K_{g}. These terms will result in nonlinear tower dynamics, causing the OCP harder to solve. Nonetheless, it can be assumed that ω_{g} varies slowly over time, such that K_{g} and ψ_i of the previous time instant, denoted $\tilde{K}_{\mathrm{g}}$ and $\tilde{\psi}_i$, are employed and do not act as decision variables of the CEMPC. Based on this assumption, the nominal side-side tower model in (10) is thus altered into the following linear dynamics

$$M\ddot{x}_{\mathrm{ss}}(t) + D\dot{x}_{\mathrm{ss}}(t) + Kx_{\mathrm{ss}}(t) = \sum_{i=1}^{B} \frac{-P_{\mathrm{r},i}(t)}{s_{\mathrm{c}}\left(\sqrt{2\tilde{K}_{\mathrm{g}}(t)/J_{\mathrm{hss}}}\Big/ G\right) R} \cos\left(\tilde{\psi}_i(t)\right), \tag{21}$$

which finalizes the model transformation for the proposed control design.

4. Convex Economic Model Predictive Control Formulation

Model predictive controllers work by calculating an optimal input trajectory such that the objectives of the plant's operation up to a certain time horizon in the future is minimized/maximized under the OCP. The first element of the generated input sequence is then fed into the plant, after which a new optimization is conducted to generate the next time step's optimal input trajectory based on new measurements—a routine known as the "receding horizon".

To formulate the objective function of the proposed CEMPC, the following requirements are considered: (i) maximize power production; (ii) alleviate structural loads; and (iii) maintain acceptable actuator activities. These requirements are thus formalized into the following economic objective function

$$\begin{aligned}\mathcal{J}_{\mathrm{OCP}}(k) = w_1 P_{\mathrm{g}}(k) + w_2 \sum_{i=1}^{B} \hat{P}_{\mathrm{av},i}(v_i(k), K_{\mathrm{g}}(k)) - w_3 K_{\mathrm{slack}}(k)^2 - w_4 \sum_{i=1}^{B} \dot{P}_{\mathrm{r},i}(k)^2 \\ - w_5 \dot{P}_{\mathrm{g}}(k)^2 - w_6 \dot{x}_{\mathrm{ss}}(k)^2,\end{aligned} \tag{22}$$

which are convex in the new variables, where k denotes the discrete time notation and w_l, with $l \in \{1, \ldots, 6\}$ being the weights on the six different objectives explained as follows. The first and second terms represent the objectives to maximize the generated power and the available aerodynamic power. The third term denotes the penalty on the rotor overspeeding with respect to the rated value by enforcing the following constraint

$$K_{\mathrm{g}}(t) \leq (J_{\mathrm{hss}}/2)\omega_{\mathrm{g,rated}}^2 + K_{\mathrm{slack}}(t), \quad \text{with} \quad K_{\mathrm{slack}}(t) \geq 0. \tag{23}$$

The fourth and fifth terms are the ROC penalties on the aerodynamic powers and the generated power and are, respectively, translated as the blade pitch and generator torque ROCs penalization. To minimize the side-side tower fatigue load, the velocity of the tower motion is penalized in the sixth term, which determines the amount of individual pitch activities to create the side-side tower force.

With the formulated linear dynamics, convex constraints, and previously-described objective function, the OCP of the CEMPC is now given by

$$\max_{\mathbf{u}_{\mathrm{t}}(\cdot)} \quad \sum_{k=0}^{N_{\mathrm{p}}-1} \mathcal{J}_{\mathrm{OCP}}(k), \tag{24a}$$

$$\text{s.t.} \quad \mathbf{x}_{\mathrm{t}}(k+1) = \mathbf{A}_{\mathrm{d}}\mathbf{x}_{\mathrm{t}}(k) + \mathbf{B}_{\mathrm{d}}\mathbf{u}_{\mathrm{t}}(k), \tag{24b}$$

$$\mathbf{x}_{\mathrm{t}}(0) = \mathbf{x}_{\mathrm{t},0}, \tag{24c}$$

$$(15),\ (17),\ (19),\ (23), \tag{24d}$$

with $\mathbf{A}_\mathrm{d}$ and $\mathbf{B}_\mathrm{d}$ as the discretized state and input matrices of the transformed wind turbine dynamics. The optimal inputs generated by the OCP, namely $P^*_{\mathrm{r},i}$ and P^*_g need to be translated back into the original variables $\beta^*_i = \Psi(v_i, K^*_\mathrm{g}, P^*_{\mathrm{r},i})$ and $T^*_\mathrm{g} = P^*_\mathrm{g} \Big/ \left(\sqrt{2K^*_\mathrm{g}(t)/J_\mathrm{hss}}\right)$, respectively, to be implementable by the wind turbine, where $\Psi(\cdot)$ denotes the pitch look-up table [9].

The initial states of the internal model in (24c) are given by either the measurements or state estimators. For this particular case, the kinetic energy value is derived from the measured generator speed while the tower states are provided by a Luenberger estimator [12] incorporating the nominal tower dynamics (10). More specifically, the side-side force estimate $\hat{F}_\mathrm{ss}$, calculated based on the wind speed, pitch angles, and rotor speed information, is fed into the Luenberger estimator together with the measured $\ddot{x}_\mathrm{ss}$, from which the tower state estimates, $\hat{\dot{x}}_\mathrm{ss}$ and $\hat{x}_\mathrm{ss}$, are obtained.

Regarding the wind speed information, it is assumed that a rotor-effective wind speed (REWS) estimate $\hat{v}_\mathrm{RE}$ is sufficient as a substitute to the blade-effective wind speeds, i.e., $v_i(k) = \hat{v}_\mathrm{RE}(k)$ for $i \in \{1, 2, 3\}$, and hence, the Immersion-and-Invariance (I&I) REWS estimator is employed. The reader interested in the detailed description of the I&I estimator is referred to [13]. For a more advanced IPC purpose, such as used for blade load mitigation, blade-effective wind speed estimates, representing more accurate spatial variability information of the wind, might be necessary [14].

5. Simulation Results and Discussions

In this section, the effectiveness of the proposed CEMPC method for the side-side tower damping is demonstrated by utilizing a high-fidelity simulation environment FAST [15], with a sampling time of 0.01 s. MOSEK optimization software [16] is employed as the numerical solver for the CEMPC, in which the prediction horizon $N_\mathrm{p} = 100$ and 0.2 s of update rate are applied. To represent modern multi-megawatt wind turbines, NREL 5 MW reference turbine [17] is incorporated as both FAST and CEMPC (internal) models. The simulation setup comprising the wind turbine, proposed CEMPC, as well as wind speed and state estimators, as explained in the previous section, are depicted in Figure 2.

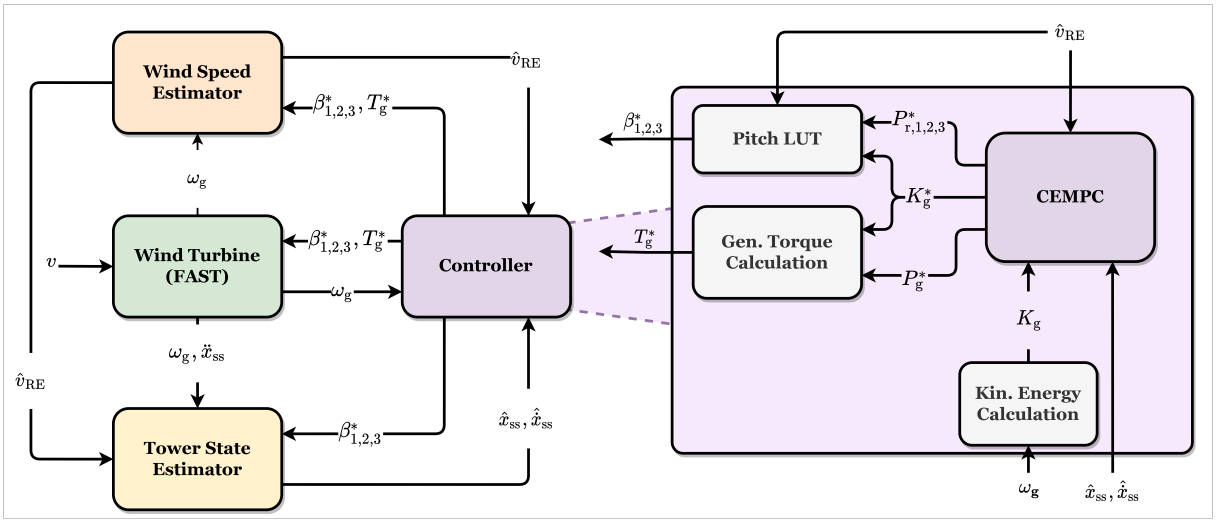

Figure 2: Convex economic model predictive control high-fidelity simulation setup.

Two cases were considered in this work: steady and turbulent wind conditions. The former is dedicated to study the trade-off of the conflicting economic objectives of the CEMPC present

in the objective function (22) and hence several sets of weights are applied and their closed-loop behaviors are compared. In the latter, the performance of the CEMPC without and with active damping by IPC is studied, where the fatigue load mitigation and the pitch actuation are evaluated by investigation of the spectral content of the measured side-side tower bending moment and pitch angle. Moreover, damage equivalent loads (DELs) of the blade bending moments, apart from that of the tower, are computed to study the effect of the proposed damping strategy on the blade loads. Finally, the impact on power production is discussed.

For both cases, only above-rated wind speeds are considered since at below-rated, maximum power production is the main goal. This means that the aerodynamic powers $P_{\mathrm{r},i}$ seek to reach their upper bounds in this region, i.e., $P_{\mathrm{r},i} = P_{\mathrm{av},i}$ and therefore, the capability to vary the side-side force becomes limited and for the remainder of this section, the evaluation at this region is not considered.

5.1. Steady Wind Case

From the objective function $\mathcal{J}_{\mathrm{OCP}}$ in (22), one may have realized that some objectives are conflicting with each other. For the side-side tower damping by IPC as considered in this work, higher damping is related to higher pitch activities, which can be detrimental to the actuators' lifetime. Hence, it can be inferred that the fourth (aerodynamic powers ROC penalty) and sixth (tower velocity penalty) terms of $\mathcal{J}_{\mathrm{OCP}}$ have some trade-offs. Several combinations of these weights, as summarized in Table 1[1], were considered and then tested under a steady wind simulation with $v = 16$ m/s to demonstrate the above points. Figure 3 depicts the closed-loop performance result of the different CEMPC weights.

Table 1: Tuning weight configurations for steady wind speed simulation.

Configuration	w_1 (-)	w_2 (-)	w_3 (-)	w_4 (s^2)	w_5 (s^2)	w_6 ($\mathrm{s}^4/\mathrm{m}^2$)
Benchmark	1	1	5	30	25	0
1	1	1	5	30	25	5
2	1	1	5	30	25	10
3	1	1	5	15	25	10

Compared with the benchmark, the first weight configuration results in an active individual pitching. The CEMPC attempts to manipulate the in-plane blade forces such that side-side tower-top force F_{ss} is created to counteract the tower excitation, reflected in a faster damping rate of the tower acceleration measurement $\ddot{x}_{\mathrm{ss}}$. When w_6 is increased, as is the case in the second configuration, the pitch becomes increasingly active, generating more F_{ss}, and even quicker damping of $\ddot{x}_{ss}$. The third configuration, which uses less aerodynamic powers ROC penalty, creates better damping with respect to the previous configuration at a cost of more pitch activities. The key takeaway of this observation is that two conflicting economic objectives of the CEMPC for side-side tower damping by IPC have been identified and confirmed, which may aid in controller tuning decisions.

5.2. Turbulent Wind Case

In this case, a realistic, extreme turbulent wind is considered with $v = 16$ m/s of mean wind speed and 14 % of turbulence intensity. The simulation was run for $t = 660$ s, in which the first 60 s

[1] It should be noted that the weight units in Table 1 differ with each other due to normalization of some objectives for numerical stability ($w_1 - w_5$), ROC penalization objectives (w_4 and w_5), and inversion of the squared acceleration unit (w_6).

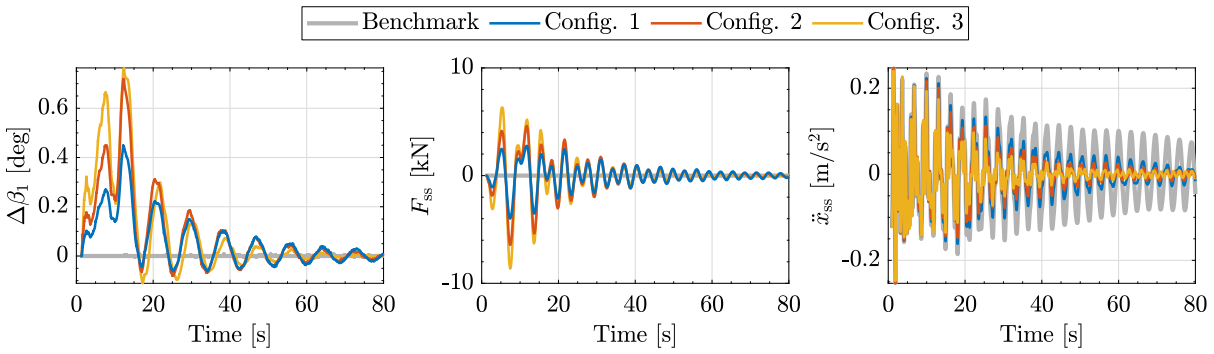

Figure 3: Time series result of steady wind speed case at $v = 16$ m/s, demonstrating the performance of the proposed convex economic model predictive control (CEMPC) under different weights (see Table 1). The left plot demonstrates the first pitch activities, only shown as its deviation from the collective component for clarity, i.e., $\Delta\beta_1 = \beta_{\text{col}} - \beta_1$. The middle plot depicts the tower-top force F_{ss} calculated by the CEMPC's internal model and the right plot shows the tower acceleration $\ddot{x}_{\text{ss}}$ measured from FAST.

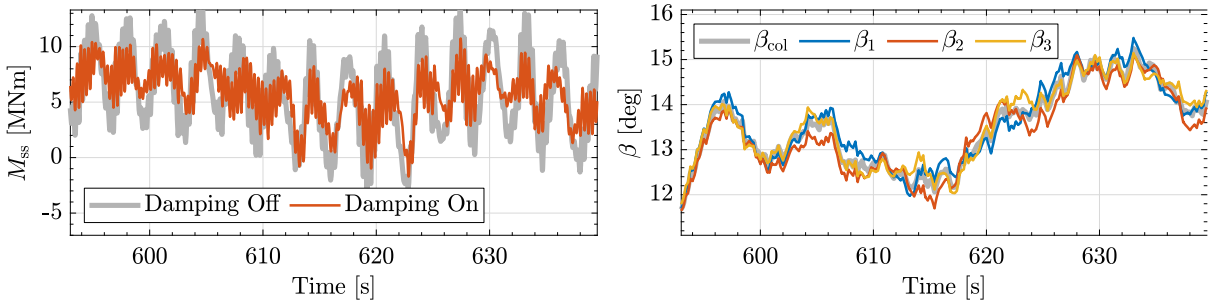

Figure 4: Time series of the side-side tower bending moment M_{ss} (left) and pitch activities (right) during the turbulent wind case.

were trimmed to remove the computational transients from the evaluation. The CEMPC without and with active damping in this case re-implement the benchmark and the third configuration of Table 1, respectively, with w_6 increased to 20 s^4/m^2 for the latter.

Figure 4 demonstrates the effectiveness of the active damping by IPC, where the side-side tower bending moment signal M_{ss} time series are shown alongside the blade pitch measurements. Significant reduction in the M_{ss} is evident thanks to the active damping by individual pitching. It can be observed that the individual pitch angles β_i, $i \in \{1, 2, 3\}$, create both steady-state offsets as well as slowly-varying component in order to damp the tower vibration, which is made more evident from the spectral analysis in the following.

In Figure 5, the power spectral density (PSD) of the tower bending moment and pitch measurements are presented. Compared with the benchmark case, the CEMPC with active damping shows reduced frequency content of the former at the tower first eigenfrequency, which is $f_{\text{twr}} = 0.32$ Hz for NREL 5 MW wind turbine. The latter, in turn, has an increased steady-state as well as $f_{\text{twr}} - f_{1\text{P}}$ frequency contents, where $f_{1\text{P}} \approx 0.2$ Hz at above-rated, which confirms the time-series observation. In theory, an increase in the $f_{\text{twr}} + f_{1\text{P}}$ frequency component should also be observed in the PSD of the individual pitch [5]. The reason why this is currently not the case is possibly due to the relatively high aerodynamic powers ROC penalty which hinders higher-frequent pitch signals to play a role. Nevertheless, since fast pitch actuation might accelerate actuator's wear, this absence could be an advantage of the current approach.

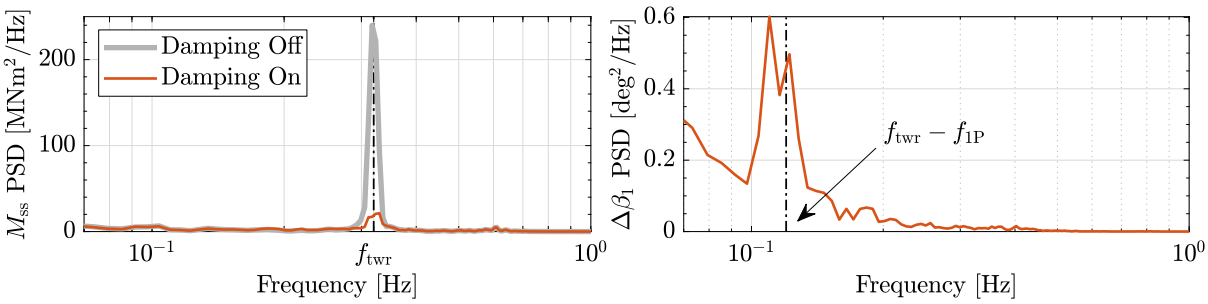

Figure 5: Power spectral density (PSD) plots of side-side tower bending moment M_{ss} (left) and first blade pitch offset from its collective component $\Delta\beta_1$ (right) for the turbulent wind case.

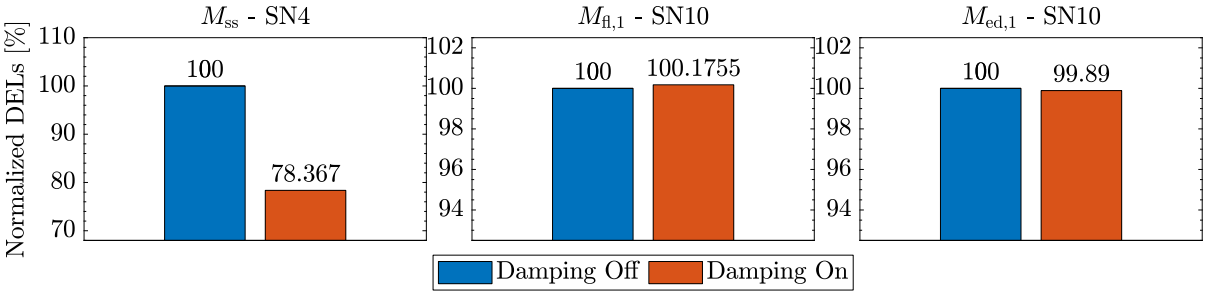

Figure 6: Normalized DELs of the side-side tower bending moment M_{ss} (left) and the flapwise (middle) and edgewise (right) bending moments of the first blade, $M_{fl,1}$ and $M_{ed,1}$, respectively.

It is also of interest to assess the fatigue damage experienced by the wind turbine components by calculating their DELs. Mainly, it is compelling to investigate not only the DEL of the side-side tower bending moment but also those of the blades as they could be impacted by the pitching activities. For the respective tower and blade materials, steel and composite are assumed; therefore, Wöhler exponent of 4 is selected for the former and 10 for the latter in DEL computation using MLife [18]. In Figure 6, the computed DELs of M_{ss}, as well as flapwise ($M_{fl,1}$) and edgewise ($M_{ed,1}$) bending moments of the first blade are depicted—normalized with respect to the benchmark results. Compared with the benchmark case, 21.633 % lower DEL of M_{ss} is obtained by the implementation of CEMPC with active damping. As for the blade, the computed DEL of $M_{fl,1}$ results in only 0.1755 % higher value, while 0.11 % lower DEL is observed for $M_{ed,1}$, with respect to the benchmark. Such little influence by the proposed method on the blade fatigue loads is likely caused by the minimum pitch activities at frequencies where these loads are dominant, i.e., at f_{1P} and its harmonics [19] (see Figure 5).

In terms of power production, 4.9827 MW of mean power is generated with 37.5088 kW of standard deviation under the CEMPC without active damping. When the damping feature of the CEMPC is turned on, a slightly higher mean power of 4.9831 MW is generated with a lower standard deviation of 36.4958 kW. Although the proposed method demonstrates better power production quality, the extent to which such improvement can be made needs further study.

6. Conclusions

In this paper, the CEMPC framework by Hovgaard, et al. [9] has been extended with IPC to mitigate the side-side tower fatigue loads of wind turbines. A variable transformation based on power and energy terms has been conducted to obtain linear dynamics and convex constraints, which enables a convex OCP to be employed. The effectiveness of the proposed method has

been demonstrated in high-fidelity simulation environment FAST at above-rated region. The conflicting economic objectives of the active tower damping, namely the tower motion and pitch actuation penalties, have been identified and validated in a steady wind case. In a turbulent wind case, the proposed method has been shown to reduce the spectral content of the side-side tower base bending moment at the tower first eigenfrequency, while the pitch spectral content at the steady-state and $f_{\text{twr}} - f_{1\text{P}}$ frequencies are increased with respect to the undamped case. Fatigue assessment of the side-side tower bending moment under active damping has shown considerable reduction in terms of DEL with negligible effects on those of the blade bending moments. Minor improvements on the power production aspect has also been observed when the IPC is active. Future work will include a comparison with a conventional baseline controller, augmentation of further load reduction objectives, such as, tower fore-aft damping and blade load mitigation, and multi-objective controller assessment.

References

[1] Enevoldsen P and Xydis G 2019 Examining the trends of 35 years growth of key wind turbine components *Energy for Sustainable Development* **50** 18–26

[2] Dykes K, Damiani R, Roberts O and Lantz E 2018 Analysis of ideal towers for tall wind applications techreport NREL/CP-5000-70642 National Renewable Energy Laboratory (NREL) Golden, Colorado

[3] Fischer B and Shan M 2013 A survey on control methods for the mitigation of tower loads *Fraunhofer IWES Report* **655**

[4] Mulders S P, Hovgaard T G, Grunnet J D and van Wingerden J W 2020 Preventing wind turbine tower natural frequency excitation with a quasi-LPV model predictive control scheme *Wind Energy* **23** 627–644

[5] Duckwitz D and Geyler M 2010 Active damping of the side-to-side oscillation of the tower *Proceedings of DEWEK*

[6] Vestas 2004 General Specification V90-3.0MW: 60 Hz Variable Speed Turbine Tech. rep.

[7] Stol K A, Zhao W and Wright A D 2006 Individual Blade Pitch Control for the Controls Advanced Research Turbine (CART) *J. Sol. Energy Eng.* **128** 498–505

[8] Rawlings J B, Angeli D and Bates C N 2012 Fundamentals of economic model predictive control *2012 IEEE 51st IEEE Conf. on Decision and Control (CDC)* (IEEE) pp 3851–3861

[9] Hovgaard T G, Boyd S and Jørgensen J B 2015 Model predictive control for wind power gradients *Wind Energy* **18** 991–1006

[10] Shaltout M L, Ma Z and Chen D 2018 An Adaptive Economic Model Predictive Control Approach for Wind Turbines *J. Dyn. Syst. Meas. Control* **140** 1–10

[11] Selvam K, Kanev S, van Wingerden J W, van Engelen T and Verhaegen M 2009 Feedback-feedforward individual pitch control for wind turbine load reduction *Int. J. Robust Nonlinear Control* **19** 72–91

[12] Schlipf D, Schlipf D J and Kühn M 2013 Nonlinear model predictive control of wind turbines using LIDAR *Wind Energy* **16** 1107–1129

[13] Liu Y, Pamososuryo A K, Ferrari R M G and van Wingerden J W 2022 The immersion and invariance wind speed estimator revisited and new results *IEEE Control Syst. Lett.* **6** 361–366

[14] Liu Y, Pamososuryo A K, Mulders S P, Ferrari R M G and van Wingerden J W 2022 The Proportional Integral Notch and Coleman Blade Effective Wind Speed Estimators and Their Similarities *IEEE Control Syst. Lett.* **6** 2198–2203

[15] Jonkman B J and Jonkman J M 2016 FAST v8.16.00a-bjj User's Guide Tech. rep. National Renewable Energy Lab.(NREL), Golden, CO (United States)

[16] ApS M 2019 *The MOSEK optimization toolbox for MATLAB manual. Version 9.0.*

[17] Jonkman J, Butterfield S, Musial W and Scott G 2009 Definition of a 5-mw reference wind turbine for offshore system development Tech. rep. National Renewable Energy Lab.(NREL), Golden, CO (United States)

[18] Hayman G 2012 Mlife theory manual for version 1.00 *National Renewable Energy Laboratory, Golden, CO* **74** 106

[19] Bossanyi E A 2003 Individual Blade Pitch Control for Load Reduction *Wind Energy* **6** 119–128